Turbulent Flows inside Pipes Equipped with Novel Perforated V-shaped Rectangular Winglet Turbulators: Numerical Simulations

M. Erfanian Nakhchi [a,1], M. T. Rahmati [a]

[a] Faculty of Engineering and Environment, Northumbria University, Newcastle upon Tyne, NE1 8ST, UK

Abstract

In this study, computational simulations have been performed to investigate the turbulent characteristics and energy consumption through heat exchanger tubes equipped by new perforated V-shaped rectangular winglet (PVRW) turbulators. The effects of the holes intensity on the velocity and temperature contours are additionally investigated. The Reynolds number, hole diameter ratio, and the number of holes are selected is in the range of $5000 \leq Re \leq 18000$, $0 \leq DR \leq 0.40$, and $0 \leq N \leq 14$, respectively. (RNG) k-ε turbulent model which is a finite volume solver is utilized for the CFD simulation. It was noticed that the proposed perforated turbulators could considerably intensify the thermal performance compared to typical VRW inserts. It is found that the recirculating flow generated by the PVRW, augments the fluid mixing and transfers the heat from the pipe walls to the core of the tube. The simulations illustrate that the amount of heat transfer enhances 25.2% with reducing the *DR* from 0.4 to 0.13 at Re=18000 and *N*=14. Also, using PVRW turbulators with *N*=7, *DR*=0.26 augments the average Nusselt number around 354.3% compared to the circular pipe without inserts. The highest thermal efficiency parameter of $\eta = 2.25$ could be obtained at Re=5000 for the heat exchangers fitted by vortex generators with *N*=14 and *DR*=0.26.

[1] Corresponding author (Mahdi.nakhchi@northumbria.ac.uk)

Keywords:

Turbulent flow, CFD, Perforated vortex generator, Rectangular winglet, Heat transfer augmentation

1. Introduction

Thermal performance augmentation plays a vital duty in the manufacturing of thermohydraulic equipment as for example, solar energy systems [1, 2], ventilation units, air conditions, and refrigeration industry. Increasing the thermal efficiency of the heat exchangers can reduce the energy costs and also the size of these systems. Besides, computational fluid dynamics (CFD) can predict the intricate flow patterns in many different turbulent boundary layer flows [3]. Several researchers conducted experimental and numerical simulations in the field of energy performance augmentation of turbulent and laminar flows by utilizing various active and passive methods, Such as twisted tapes [4-6], ribbed and corrugated channels [7-9], wavy surfaces [10, 11], conical rings [12], louvered strips [13], hollow cylinders [14], asymmetric sinusoidal channels [15, 16], nanofluids [17-21], baffle turbulators [22-24], helical screw tapes [25, 26], rotating two-pass channels [27] and triangular obstacles [28].

Winglet vortex generators are one of the most popular heat transfer improvement tools which are widely used in many different thermal systems. Many investigators performed experimental and numerical works on the thermohydraulic efficiency of the heat exchanger tubes equipped by various winglet vortex generators. Experimental research was performed by Zhou and Ye [29] on the thermal efficiency and characteristics of turbulent flows inside pipes fitted by curved trapezoidal winglet vortex generators. They observed that small attacks-angle of the turbulator (β = 0° and 15°), have higher thermal performance in comparison with larger attack angles. Wu and

Tao [30] examined the effects of delta-winglets VG on thermohydraulic efficiency augmentation on finned-tube surfaces by two tube rows. Their CFD simulations revealed that the winglets could considerably enhance the heat transfer rate and decrease the friction loss by optimizing the size and geometry of the delta winglets turbulators. It was concluded that that the average Nu number could be increased 17–21% compared with typical fin-tube surfaces under the same Reynolds numbers. Gholami et al. [31] presented a numerical analysis of the effects of wavy rectangular winglet VGs on thermal performance augmentation of compact heat exchanger tubes. The Reynolds number was in the range of 400 to 800 in their investigations. They illustrated that the "wavy-up" rectangular winglets have more influence on the thermal performance enhancement compared to wavy-down ones. Song et al. [32] experimentally determined the forces of curving winglets vortex generator inside heat exchanger tubes under relatively low Reynolds numbers. They revealed that smaller VGs which was located close to the pipe, perform better than the other cases at low Re numbers. Xu et al. [33] numerically investigated the effects of WVGs on thermal performance augmentation inside circular pipes. The fluid flow was assumed to be fully turbulent ($6000<Re<33000$) and constant wall heat flux was imposed on the walls. Their simulations showed the case with B=0.1 has the highest thermohydraulic performance factor (TPF) because of the lower friction factor compared with the other test case. The maximum performance parameter of 2.0 was obtained for PR=1.0 with the BR=0.15 case. Other researchers also performed numerical and experimental investigations on various winglet vortex generators in different thermal engineering systems such as wavy delta winglets [34].

Recently, the use of perforated turbulators has become a popular method for improving thermal efficiency and reducing pressure loss in heat exchangers [35]. Perforated vortex generators are popular in the design of thermal energy systems. They can easily be made by employing

perforated metal sheets to manufacture various types of perforated turbulators. Using perforated surfaces can significantly augment the fluid mixing which improves the turbulent flow characteristics inside industrial equipment. Luo et al. [36] proposed novel solar heat exchangers by employing the combination of grooves and delta-winglet vortex turbulators. The conclusions revealed that a combination of DWVGs and ribs improves the thermo-hydraulic performance of the solar system around 22%. Skullong et al. [37] studied numerically and experimentally the turbulent flow characteristics and thermal efficiency in solar heaters fitted by penetrated winglet vortex generators. They observed that vortex generators with a hole diameter of d=1mm have higher heat transfer rates compared with larger hole diameters. They found that the average Nusselt number was about 6.78 times over the plain duct. The highest thermal performance of 2.01 was obtained for the penetrated winglets with a hole diameter of 5 mm. The number and the position of the holes remained constant in their study. Chamoli et al. [38] carried out a numerical and experimental analysis on turbulent flows and thermal performance inside the tubes equipped by perforated turbulators. They reported that the thermal enhancement parameter of 1.65 could be reached at Re=3,000 with perforated index (PI) of 16%. Two correlating equations for Nu number and friction loss were also developed in their study as based on the physical and thermal design parameters.

Nakhchi and Esfahani [12] used perforated conical rings through the heat exchangers with the turbulent flow regime. They employed Cu-water nanofluid as the working fluid. Their numerical analysis showed that the highest thermo-hydraulic enhancement parameter of 1.10 was obtained by utilization of conical ring with ten holes ($N = 10$) at $\mathrm{Re} = 5{,}000$. The effects of perforated rings on the thermal efficiency of double-pipes heat exchangers was numerically and experimentally evaluated by Sheikholeslami and Ganji [39]. They reported that $\eta = 1.59$ can be

obtained by employing rings with perforations and PR=1.06 with an open area ratio (λ) of 0.07 at Re=6000. Nakhchi et al. [13] numerically examined the turbulent flow characteristics in heat exchangers fitted by perforated louvered strip inserts. It was observed that the perforations play a significant role in vortex generation and thermal performance enhancement inside thermal systems. Recently, Promvonge and Skullong [40] conducted an experimental analysis on the thermal efficiency of heat exchangers pipes by using novel V-shaped rectangular winglet turbulators. They employed V-shaped turbulators with four winglets pitch ratios ($0.5<PR<2.0$) and three winglets blockage ratios ($0.1<BR<0.2$) with a constant attack angle (45^{o}). The results revealed that thermal performance could significantly be improved by using V-RW vortex generators.

The above literature survey illustrates that among various numerical and experimental investigations in the field of vortex generators, the recent experimental study of Promvonge and Skullong [40] on rectangular winglet vortex generators showed much higher thermal performance factor compared to previous ones. Besides, using perforated turbulators is a powerful and efficient method for improving the thermo-hydraulic enhancement parameter of heat exchanger systems. This motivated us to numerically investigate the fluid flows and heat transfer through heat exchangers improved by rectangular V-shaped winglet turbulators (PRVW) with and without perforations to understand better the physical reasons of heat transfer augmentation near these new vortex generators. To the best of the authors' knowledge, no numerical or experimental investigations have been performed on rectangular V-shaped vortex generators with perforations. In this study, turbulent flow characteristics such as flow streamlines, velocity and temperature contours and other physical parameters will be discussed

in detail. The influences of the number of holes on the thermal efficiency parameter of the system will also be provided.

2. Physical model

Figure 1 depicts the schematic view of a circular pipe equipped by perforated V-shaped rectangular winglet (PVRW) turbulators. After passing through the inlet section, the cold air flow enters the main heat exchanger tube which is heated with uniform wall heat flux. The tube length (L=1200mm) and the tube diameter (D=50.8mm) are kept constant at 1200mm and 50mm, respectively. The number of holes (N) and holes diameter (d) are in the range of 0-14 and 1-3 mm, respectively. The descriptions of the geometrical parameters are also depicted in Fig. 1. The PVRW turbulators are mounted on a flat tape with 0.5mm thickness. The turbulators and the tape are made of aluminum. The pitch between the vortex generators along the pipe is constant at 50 mm. The design parameters are selected according to the experimental work of Promvonge and Skullong [40] for better comparison with experimental data. Based on the experiments, the vortex generators with width (b) of 7.5 mm perform better than the other geometries. Therefore, b= 7.5 mm is utilized for the computational analysis to investigate the effect of perforations on the energy transmission, friction loss, and thermohydraulic efficiency of the system. The dimensions of the design parameters are presented in Table 1. The air inlet velocity (u_{in}) is constant and the Re number ($Re=u_{in}D/\nu$) is between 5,000 and 18,000. The inlet temperature is presumed to be 300K and the PVRW turbulators are adiabatic and zero slip BCs are presumed on both of the pipe surfaces and PVRW vortex generators.

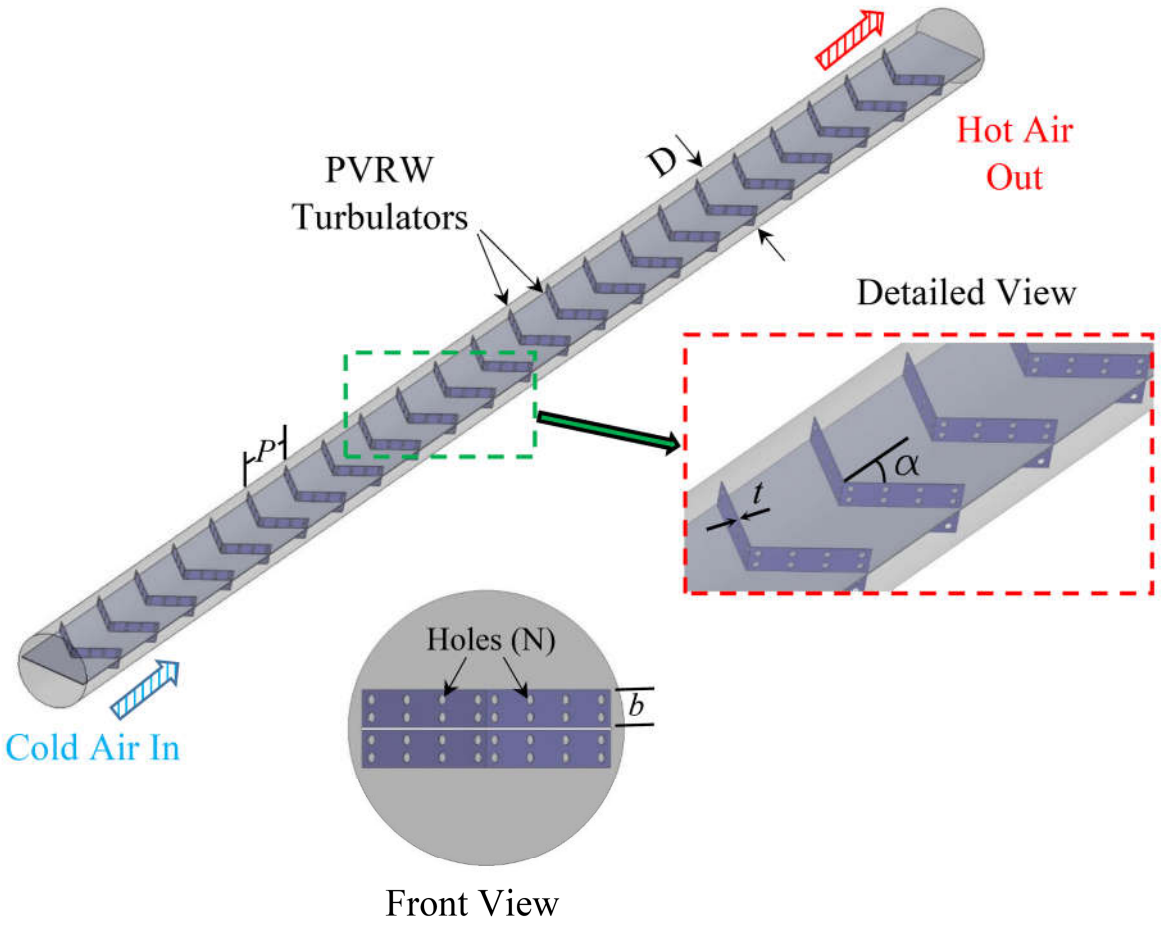

Fig. 1 Schematic view of heat exchanger pipe equipped by PVRW turbulators

Table 1 Dimensions of the design parameters inside heat exchanger pipe equipped with PVRW vortex generators

Parameter	**Symbol**	**Value**
Inlet section	*(L_i)*	1500 mm
Duct length	*(L)*	1200 mm
Duct diameter	*(D)*	50.8 mm
Slant angle	*(α)*	45°
PVRW width	*(b)*	7.5 mm
Number of holes	*(N)*	0, 7, 14

Holes diameter	*(d)*	1, 2, 3 mm
PVRW thickness	*(t)*	0.3 mm
Plate width	*(w)*	50 mm
Pitch	*(P)*	50 mm
Tape thickness	*(δ)*	0.5 mm
hole diameter ratio	*DR=d/b*	0.13, 0.26, 0.4
Reynolds number	Re	5000-18000

The geometries of the test cases in the present work are depicted in Fig. 2. Heat transfer and turbulent flow inside tubes equipped by typical WVGs without perforations are also investigated for a better understanding of the characteristics of the turbulent flow near the vortex generators.

a) Plain tube

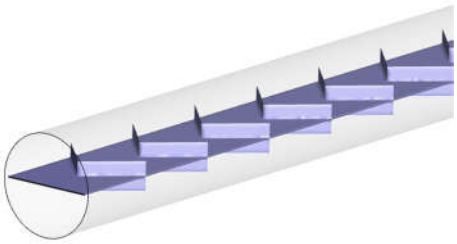

b) *N*=0 (Conventional WVG)

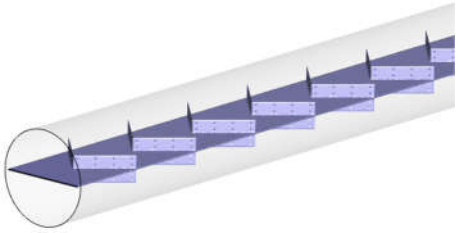

c) *N*=8, *DR*=0.13

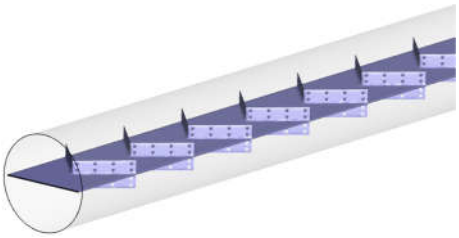

d) *N*=8, *DR*=0.26

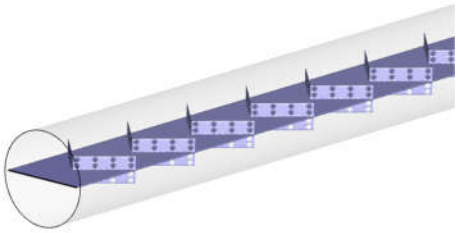

e) *N*=8, *DR*=0.4

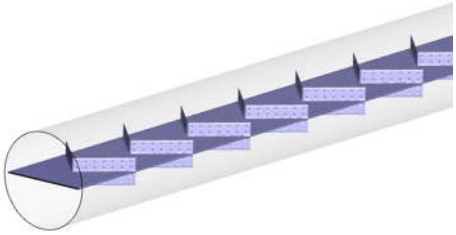

f) *N*=14, *DR*=0.13

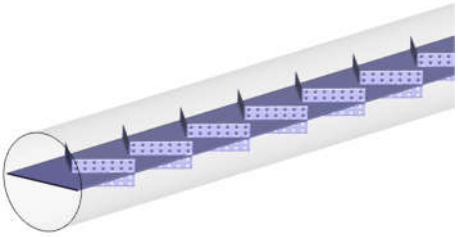

g) N=14, DR=0.26

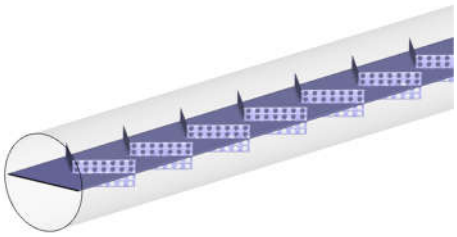

h) N=14, DR=0.4

Fig. 2 The schematics of the test cases in the present study

3. Mathematical modeling

The turbulent flow is presumed to be three dimensional, incompressible, and steady. The governing equations in the tensor form can be expressed by [5]:

$$\frac{\partial}{\partial x_i}\left\langle \rho u_i \right\rangle = 0 \tag{1}$$

$$\frac{\partial}{\partial x_j}\left\langle u_i \rho u_j \right\rangle = \frac{\partial}{\partial x_j}\left(-\rho\overline{u_i' u_j'}\right) - \frac{\partial p}{\partial x_i} + \frac{\partial}{\partial x_j}\left\{\mu\left[\frac{\partial u_i}{\partial x_j} + \frac{\partial u_j}{\partial x_i}\right]\right\} \tag{2}$$

$$\frac{\partial}{\partial x_j}\left\langle \rho T u_i \right\rangle = \frac{\partial}{\partial x_i}\left\{\frac{\partial T}{\partial x_i}\left(\frac{\mu}{\mathrm{Pr}} + \frac{\mu_t}{\mathrm{Pr}_t}\right)\right\} \tag{3}$$

where $\mu_t = \rho C_\mu \dfrac{k^2}{\varepsilon}$ is the turbulence viscosity. $\rho\overline{u_i' u_j'}$ term can be evaluated by [41]

$$\rho\overline{u_i' u_j'} = \mu_t\left(\frac{\partial u_i}{\partial x_j} + \frac{\partial u_j}{\partial x_i}\right) - \frac{2}{3}\rho k\,\delta_{ij} - \frac{2}{3}\mu_t\frac{\partial u_k}{\partial x_k}\delta_{ij} \tag{4}$$

k and ϵ equations of the turbulent model are [41]

$$\frac{\partial}{\partial x_i}\left\langle \rho u_i k \right\rangle = \frac{\partial}{\partial x_j}\left[\left(\frac{\mu_t}{\sigma_k} + \mu\right)\frac{\partial k}{\partial x_j}\right] - \rho\epsilon + G_k \tag{5}$$

$$\frac{\partial}{\partial x_i}\left\langle \rho u_i \epsilon \right\rangle = \frac{\partial}{\partial x_j}\left[\frac{\partial \epsilon}{\partial x_j}\left(\frac{\mu_t}{\sigma_\epsilon} + \mu\right) + \frac{\epsilon}{k}\left(C_{1\epsilon}G_k - \rho C_{2\epsilon}\varepsilon\right)\right] \tag{6}$$

Where $G_k = -\rho\overline{u_i'u_j'}\frac{\partial u_j}{\partial x_i}$. The turbulent model fixed terms are:

$$\begin{aligned} C_{1\varepsilon} &= 1.42 \quad \Pr_t = 0.85 \quad C_\mu = 0.084 \\ C_{2\varepsilon} &= 1.68 \quad \sigma_k = 1 \quad \sigma_\varepsilon = 1.3 \end{aligned} \tag{7}$$

ANSYS ICEM 19.2 software was employed for grid generation. Fig. 3 shows the grid that is used for the CFD simulations. It can be observed that an inflation mesh is employed near the pipe surface to calculate the viscous sublayer influence accurately. The tetrahedral mesh is employed inside the tube, and smaller grid elements are selected near the PVRW vortex generators to capture the recirculating flows in these areas. The maximum element size was chosen to be less than 0.1 mm near the PVRW turbulators. The y+ value remained less than one on both of the tube walls and the turbulators.

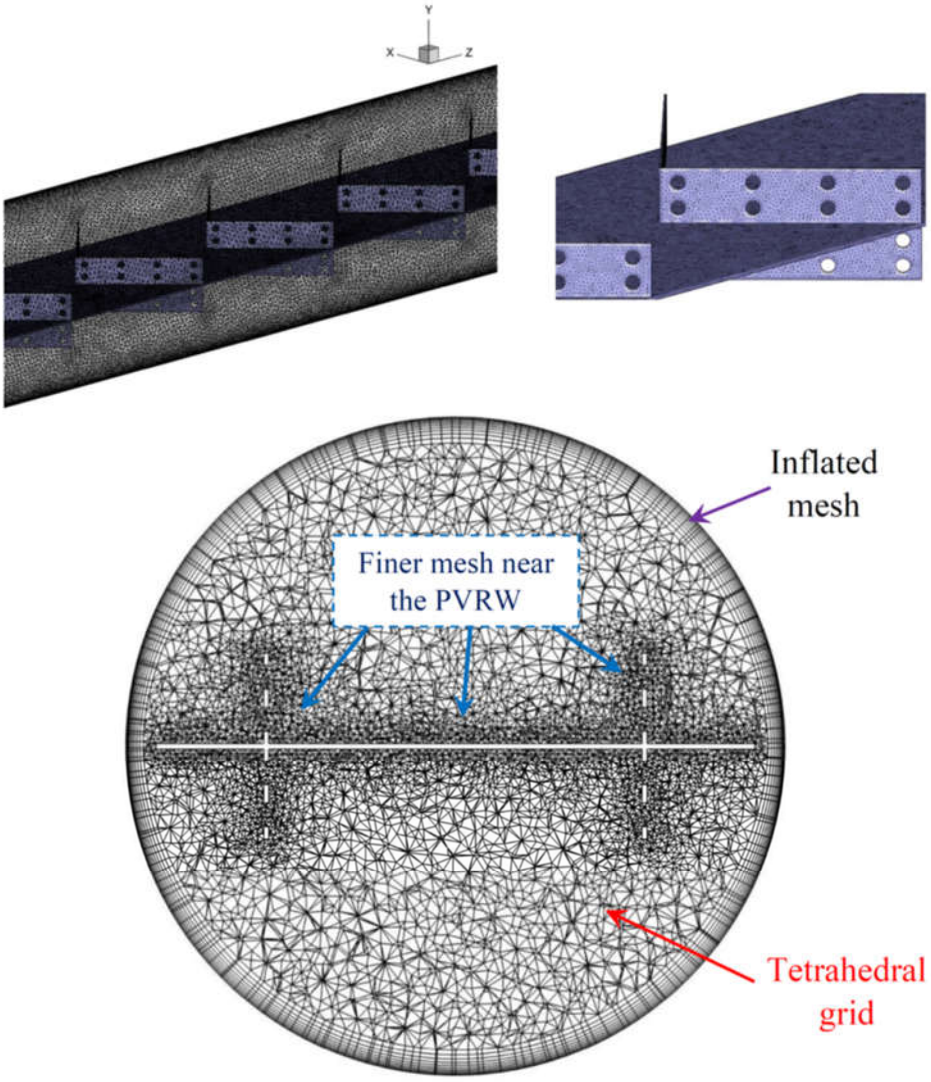

Fig. 3 Typical mesh used in the computational domain.

The CFD simulations for the heat exchanger pipe fitted by PCRW insert were performed by using the finite volume technique. The turbulent flow equations were solved by ANSYS Fluent 19.2 software by employing the SIMPLE algorithm solver. The second-order upwind scheme was utilized for Navier Stokes equations discretization. Several RANS models (k- ε, k-ω, SST-k-ω and Renormalization Group k- ε models) were employed and the results of each model were compared to the empirical results existing in the literature. Between the turbulent models, the

RNG k-ϵ model has more precise results compared with the experimental data (Fig. 4). Therefore, it was selected for further studies. The continuity, momentum, k and ϵ equations were presumed to meet the convergence criteria when the residuals were less than 10^{-5} and that of the energy equation was smaller than 10^{-7}.

3.1. Data reduction

The following dimensionless parameters are selected for evaluating the heat transfer rate and friction loss of turbulent airflow inside the tubes fitted with PVRW inserts: Re and Nu numbers, friction parameter, and the thermal efficiency factor. Re, Nu, and *f* are defined as:

$$\mathrm{Re} = \frac{uD}{\nu} \tag{8}$$

$$Nu = \frac{hD}{k} \tag{9}$$

$$f = \frac{\Delta P}{\rho u_i^{\,2}} \frac{2D}{L} \tag{10}$$

As thoroughly discussed in the recent work of Promvonge and Skullong [40], instead of the well-known thermal performance equation $\left(\eta_{\mathrm{old}} = \left(Nu / Nu_s\right) / \left(f / f_s\right)^{1/3}\right)$, it is more accurate to use the following novel proposed equation, which is developed based on equal pumping power.

$$\eta_{\mathrm{new}} = \frac{\left(Nu / Nu_s\right)}{\left(f / f_s\right)^{1/3}} \cdot \left(f / f_s\right)^{7/165} = \eta_{\mathrm{old}} \cdot \left(f / f_s\right)^{7/165} \tag{11}$$

In the present study, this new equation is employed for calculation of the thermal performance factor, which gives a slightly higher thermal efficiency in comparison with the old equation.

3.2. Grid independence study

To perform the grid independency study, the average heat transmission rate and friction loss of turbulent airflow inside the pipe enhanced by PVRW turbulator at Re = 18,000, N=14, DR =0.4 (extreme case) were calculated for four different element numbers. The details are provided in Table 2. The results illustrate that the heat transfer augments by increasing the Reynolds number while the friction loss is decreased. The trends of the friction factor variations with the inlet velocity of turbulent flow are similar to the Moody-chart. As can be observed, 925290, 1287036, 3991581, and 7584125 elements were employed for the CFD analysis. It was observed that the deviation of Nu and f between 3991581 and 7584125 mesh numbers are 0.45% and 0.20%, respectively. Therefore, 3,991,581 elements, including tetrahedral elements inside the channel and inflated grid near the walls, were selected for the numerical computations.

Table 2 Grid independence study for PVRW turbulator at Re = 18,000, N=14, DR =0.4.

Number of elements	Nu	deviation %	f	Deviation %
925,189	126.87	-	0.357	-
1,287,036	159.42	25.65	0.446	24.92
3,991,581	173.29	8.70	0.494	10.76
7,584,125	174.08	0.45	0.495	0.20

3.3. Code validation

To validate the CFD results, the Nusselt numbers and pressure loss coefficients for both of the circular pipe and the pipes equipped by typical V-shaped rectangular winglet (VRW) turbulators are validated with the experimental data of Promvonge and Skullong [40] for several Reynolds numbers. It is observed that the numerical simulations have small deviations with the experiments, which means that the turbulent model and the solution method are selected

appropriately for the numerical simulations based on the FV method. It also should be pointed out that the CFD computations are also in agreement with previous experiments for turbulent air flows inside circular tubes without inserts.

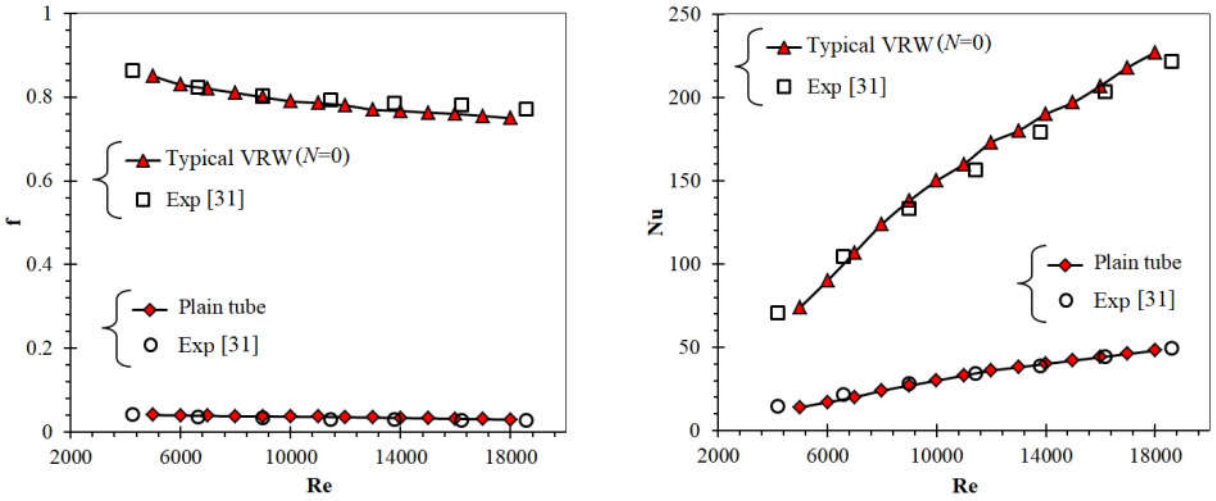

a) Friction loss b) Average Nu number

Fig. 4 Validation of numerical simulations for typical VRW vortex generators with experimental data

4. Results and discussion

Fig. 5 depicts the flow streamlines as functions of the turbulent axial velocity inside a circular tube and the heat exchanger tube augmented by PVRW vortex generators with N=8, DR=0.26 at the Reynolds number of 10,000. It can be observed that the perforated V-shaped vortex generators cause strong recirculating flows between the duct walls and the tube center. The perturbations intensify the fluid mixing, which results in a higher heat transfer rate compared to a pipe without any insert. The results illustrate that the axial velocity of turbulent flow near the leading edges of the vortex generators is relatively higher than the other areas. Physically speaking, the strong current through the holes of the PVRW inserts is one of the main reasons for

the flow disturbance near the turbulators which are fitted on the flat tape in the middle of the duct.

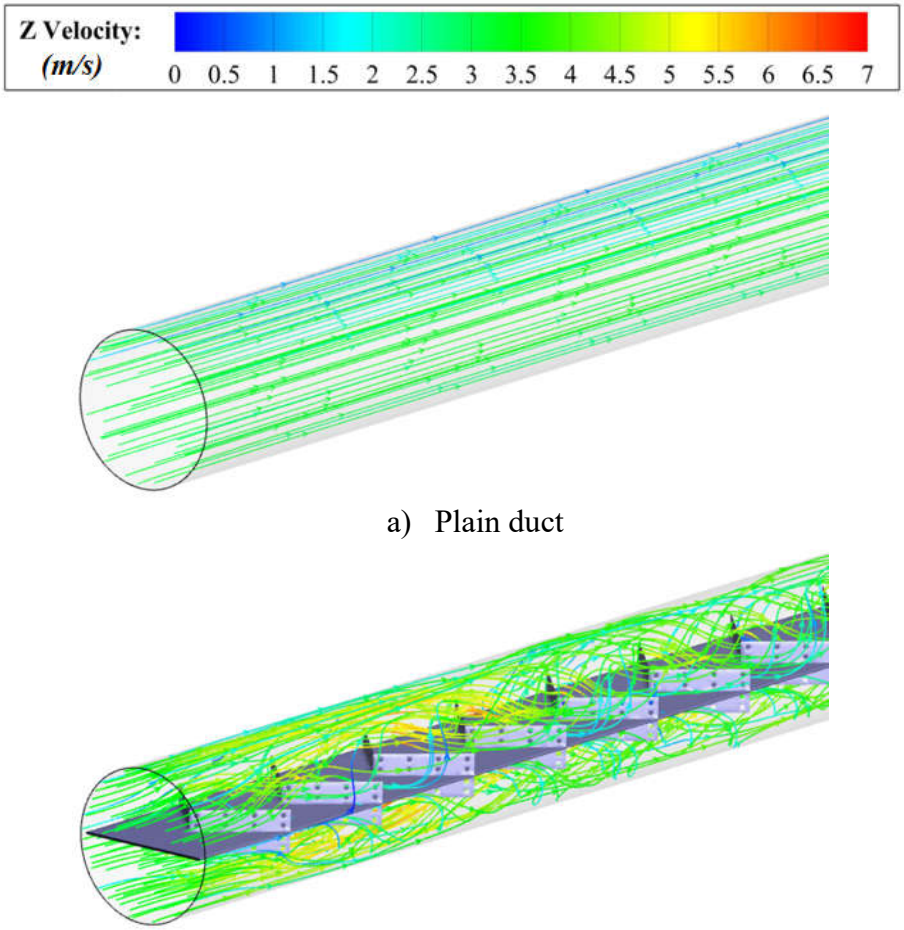

a) Plain duct

a) Tube fitted with PVRWs with N=8 and DR=0.26

Fig. 5 Flow streamlines inside plain duck and the tube equipped by PVRW turbulators with N=8, DR=0.26 at Re=10,000.

Axial velocity contours of turbulent airflow inside typical VRW and PVRW turbulators with different geometries are shown in Fig. 6. It can be observed that in the backward direction of all of the turbulators (blue areas) vortex flow is generated. However, in the top and bottom leading edges of PVRW inserts, the axial velocity is much higher than the other regions. This strong axial flow may be one of the main physical reasons for boundary layer disruption. As expected,

the vortex generation, reduced by using perforated turbulators instead of the typical ones. The results show that the vortex generation becomes smaller by increasing the number and the diameter of the holes.

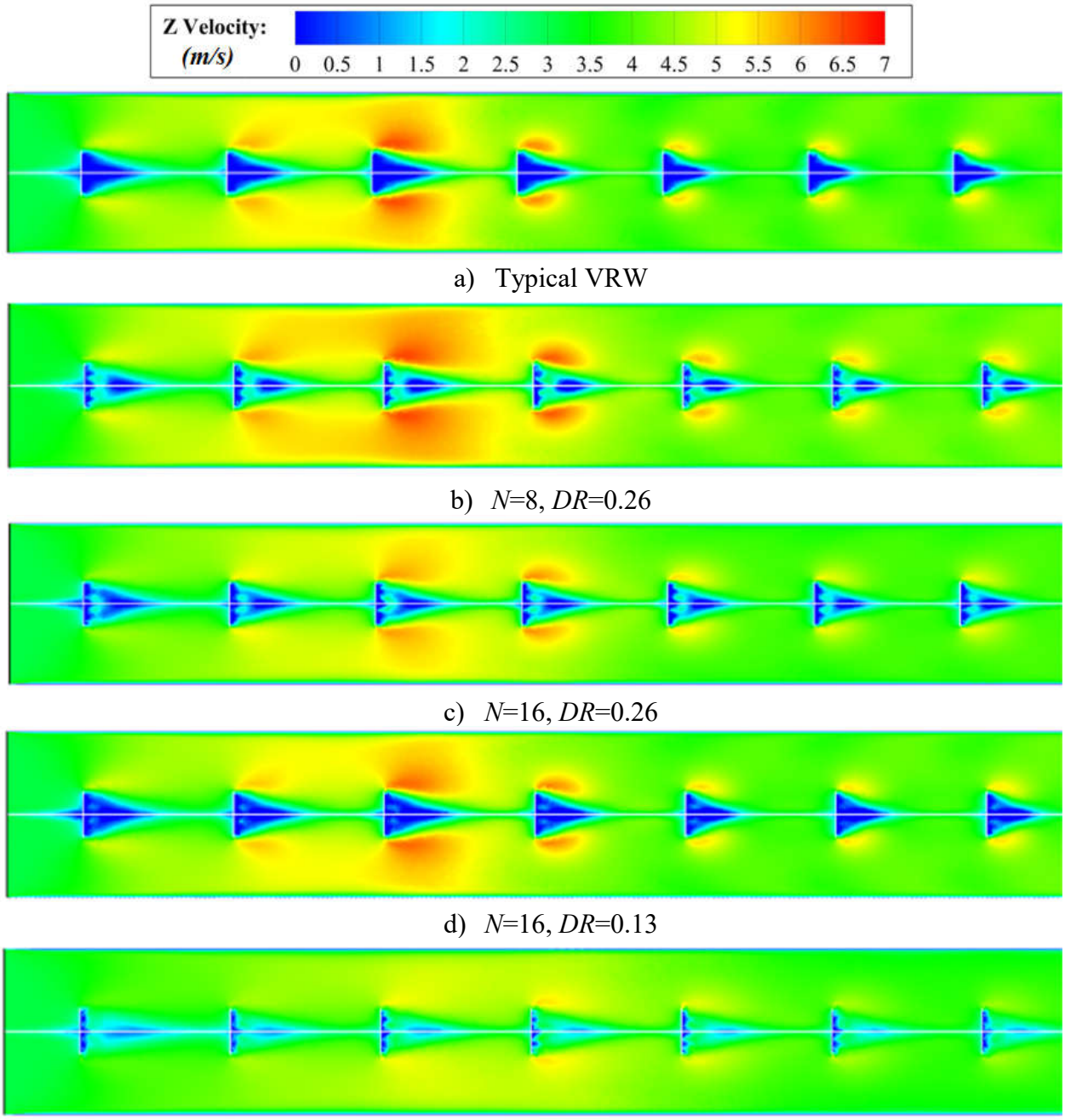

a) Typical VRW

b) N=8, DR=0.26

c) N=16, DR=0.26

d) N=16, DR=0.13

e) N=16, DR=0.4

Fig. 6 Contours of turbulent axial velocity in the heat exchangers fitted by typical VRW and PVRW inserts at Re =10000.

Figure 7 shows the turbulence kinetic energy contour with tangential velocity vectors at 3 different axial cross-sections (z=0.2, 0.24 and 0.28 m) of turbulent airflow through the heat exchangers equipped by VRW vortex generators at Re=10,000. The details of the tangential flow streamlines are also provided. It can be seen that the recirculating flow generated by the VRW, improves the fluid mixing and transfers the heat from the heated walls to the center of the duct. It could be seen that some vortex flows are also generated inside the heat exchanger tube which intensifies the TKE rate. The intense kinetic energy besides the leading edges of the VRW turbulator at z=0.2 m is one of the essential physical reasons for heat transfer improvement in the existence of vortex generators.

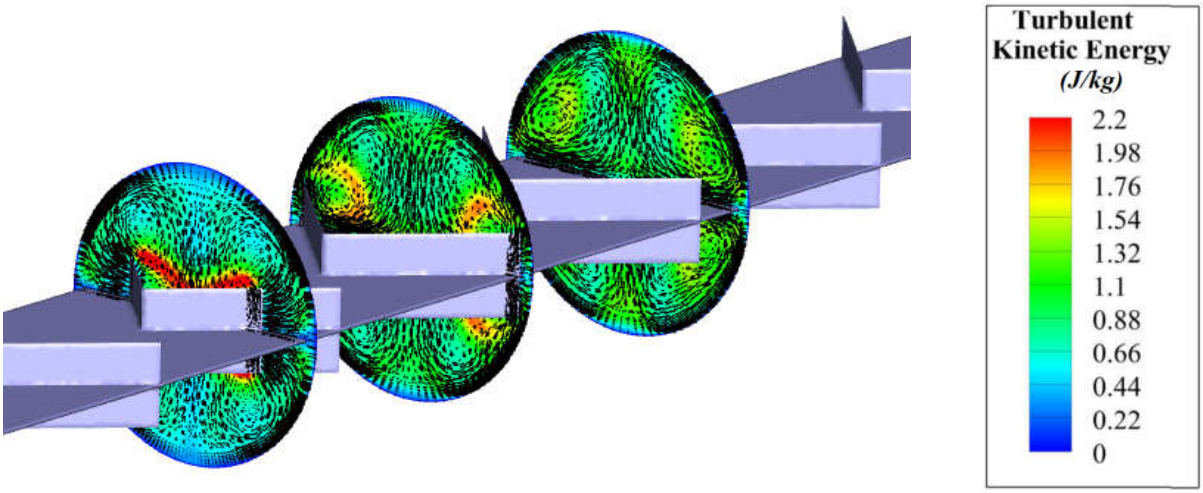

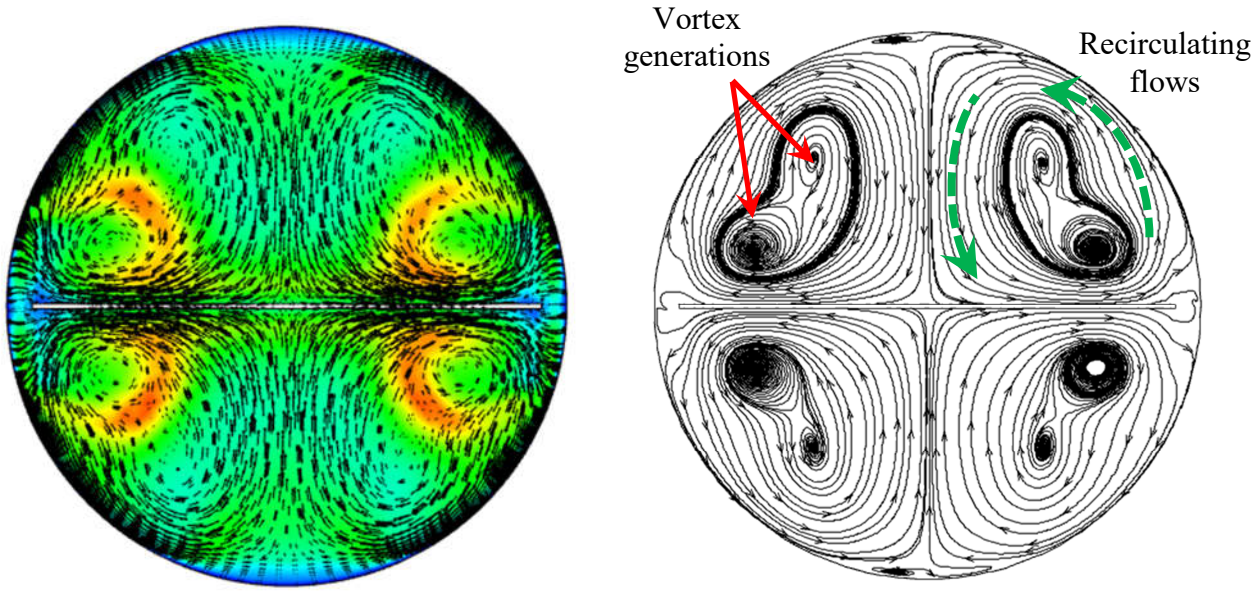

Detailed view at z=0.2 m Surface flow streamlines (z-0.2 m)

Fig. 7 Tangential velocity vectors, TKE contours, and surface flow streamlines inside the duct fitted by VRW inserts at Re=10000.

Fig. 8 illustrates the TKE contours in the axial direction for various perforated V-shaped rectangular winglet vortex generators with uniform inlet velocity. The Reynolds number is selected to be 10,000, and the results were compared with the plain duct. It can be observed that the TKE value for typical VRW inserts is the highest among the tested geometries. As discussed earlier, this is mainly because the perforations reduce the vortex flows in the backward direction of the turbulators. However, the holes can significantly reduce the pressure drop of turbulent flow in heat exchangers ducts. The results illustrate that the severe kinetic energy considerably decreases by using perforated V-shaped rectangular winglet inserts with larger diameter ratios. Increasing the diameter of the perforations can reduce the recirculation flows between the duct walls and the core area.

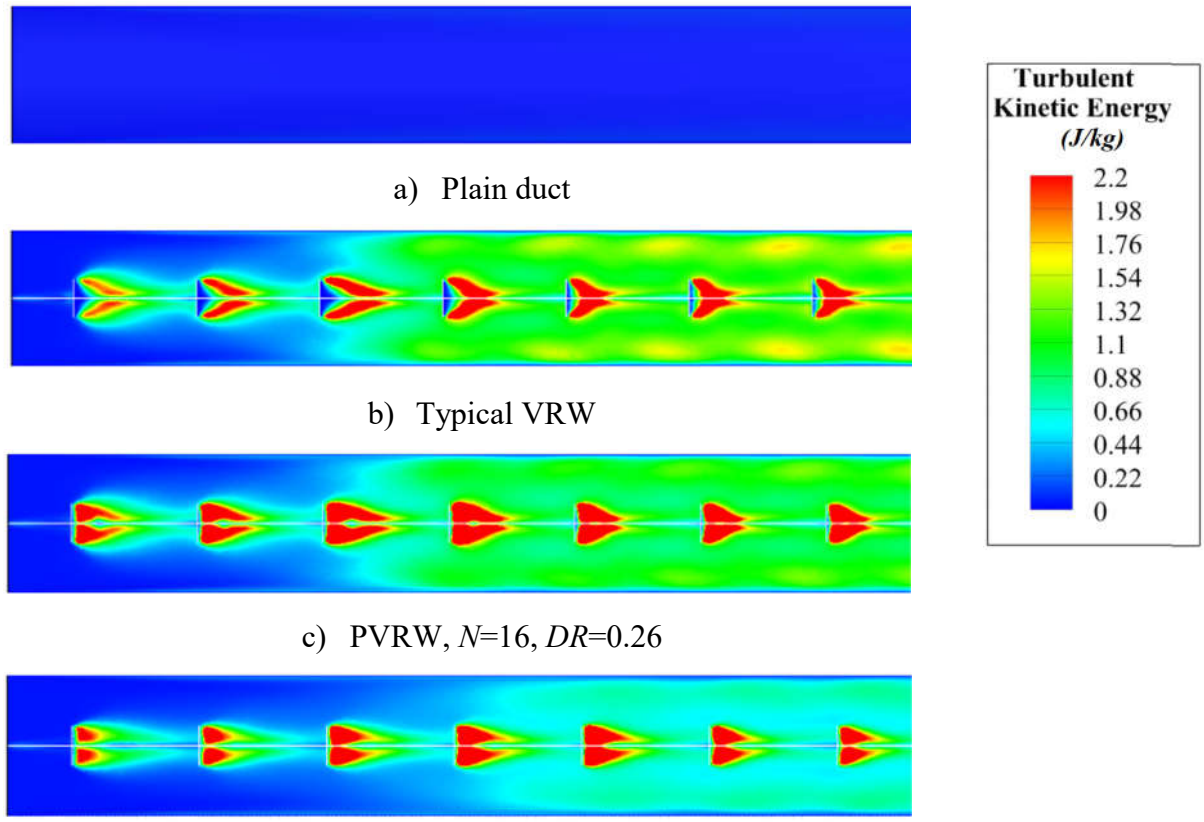

a) Plain duct

b) Typical VRW

c) PVRW, N=16, DR=0.26

d) PVRW, N=16, DR=0.4

Fig. 8 TKE contours of fluid flows in heat exchanger ducts improved by different perforated inserts at Re=10,000.

The temperature distributions of turbulence air flows in the heat exchanger pipes fitted with typical VRW insert and perforated ones in five different cross-sections are presented in Fig. 9. As expected, V-shaped rectangular winglet turbulators significantly make better the heat transfer rate compared with a typical tube. The contours show that the temperature enhancement for typical VRW insert is better than the perforated VRWs, which are in agreement with previous arguments regarding the more efficient vortex flows in the presence of typical VRW turbulators. It can be seen that the temperature of the airflow decreases by raising the number of perforations from 8 to 14 which is due to the reduced vortex generation in the presence of more perforations.

It also can be deduced that the temperature augmentation of the turbulent flow for (N=16, DR=0.40) model is the smallest among the tested geometries.

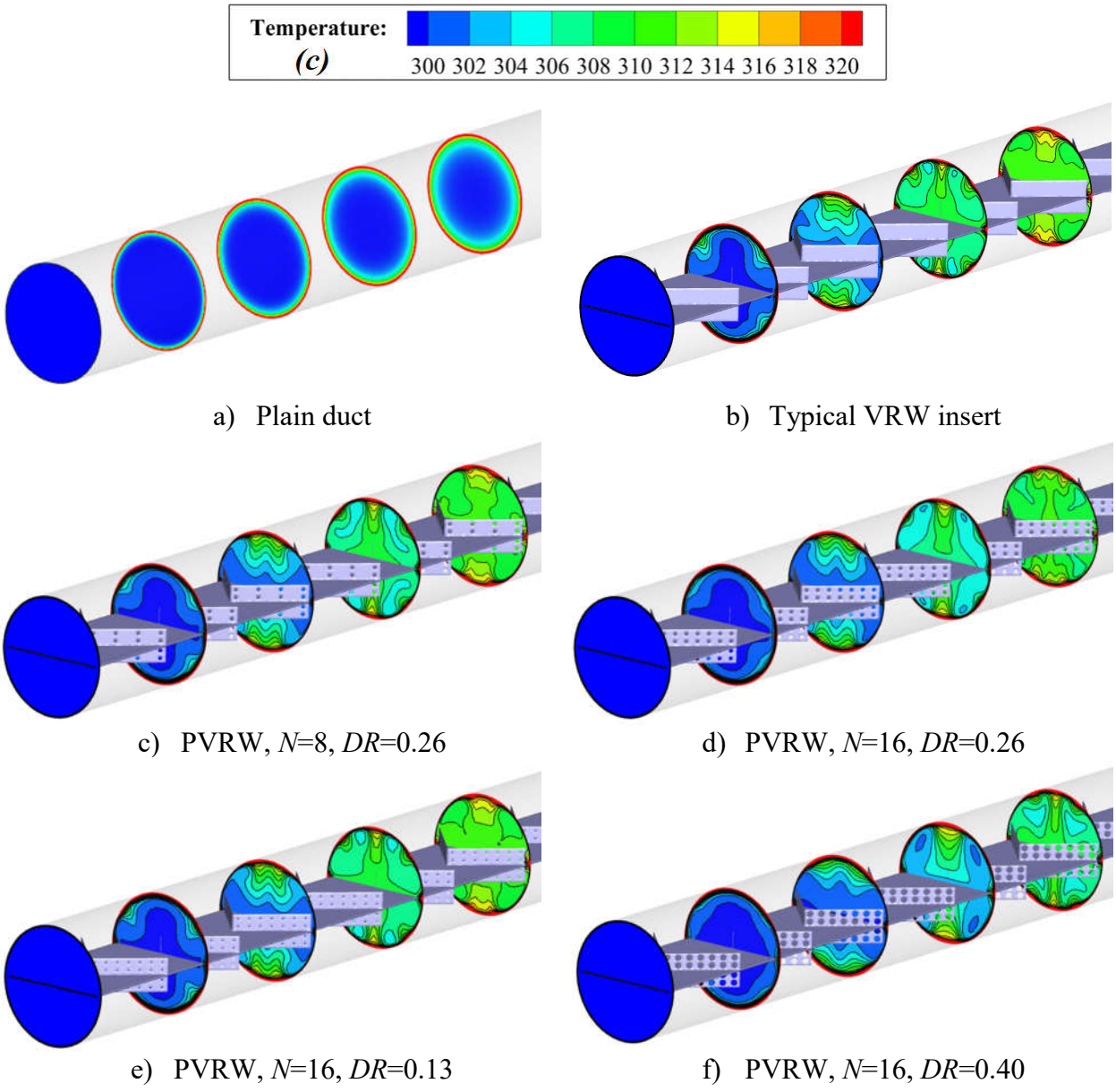

Fig. 9 Temperature contours of turbulent flows through the plain duct and the heat exchanger pipes equipped by different perforated VRWs at Re=10,000.

Figure 10 shows the Nusselt number values versus the Re number for different V-shaped rectangular winglet VGs. The results illustrate that the heat transfer measure is maximum for the case of a typical VRW insert without perforations (N=0), which is consistent with the physical arguments provided for Figure 8. The principal cause for heat transfer intensification is the recirculating flows amongst the tube surface and the core region. The graph illustrates that the Nusselt number augments by raising the axial velocity. This augmentation is because of the boundary-layer disruptions near the heat exchanger wall at higher turbulent inlet velocities. The heat transfer rate decreases about 66% by raising the number of holes from 0 to 14 with similar diameter ratios. The vortex generation reduces by raising the number of perforations and increasing their diameters. The results demonstrate that the Nu number improves by 25.2% with reducing the DR from 0.4 to 0.13 at Reynolds number of 18000 and N=14. The numerical results reveal that using PVRW inserts with N=7, DR=0.26, augments the average Nusselt number around 354.3% compared with the simple plain tube without inserts. The highest Nu number of 227.18 is obtained by employing typical VRW inserts without holes (N=0) through the heat exchanger tubes at the Reynolds number of 18000.

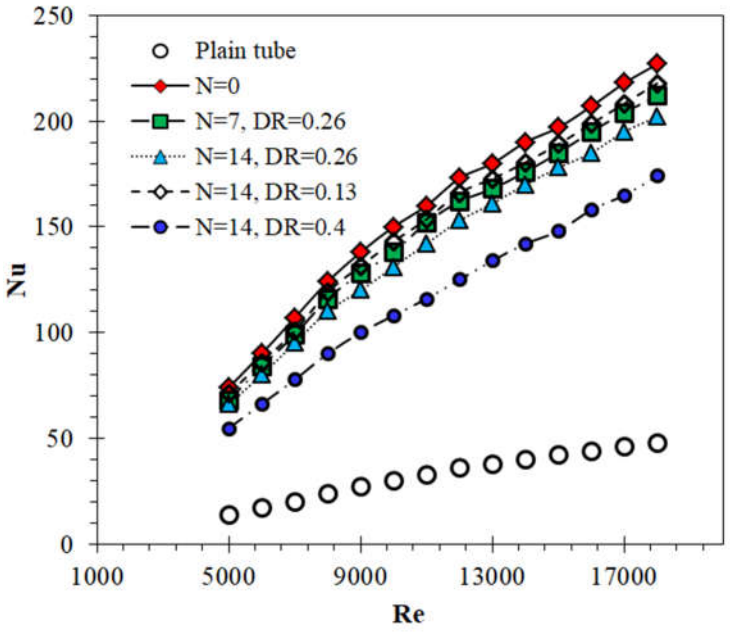

Fig. 10 Variations of Nu number by Re number for various PVRW turbulators with various geometries

Fig. 11 shows the changes in the friction loss to the Re number for various V-shaped rectangular winglet vortex generators. The results illustrate that the friction loss is reduced by raising the Re number, which is in agreement with the Moody diagram data for turbulent flow. It also can be observed that using perforated turbulators instead of typical VRW inserts could significantly reduce the pressure drop of the turbulent flow through the heat exchanger pipe. It is visible that the friction factor reduces by 26.1% with increasing the number of perforations from 0 to 14 at Re=10,000 and *DR*=0.26. Besides, the friction factor augments up to 51.5% compared to the circular duct without an insert. Using PVRW inserts enhances the viscous loss effects of the air flows close to the pipe wall and as a result, the friction loss increases. It should be pointed out that another important physical cause for friction loss intensification is recirculation flow among the duct walls and central regions.

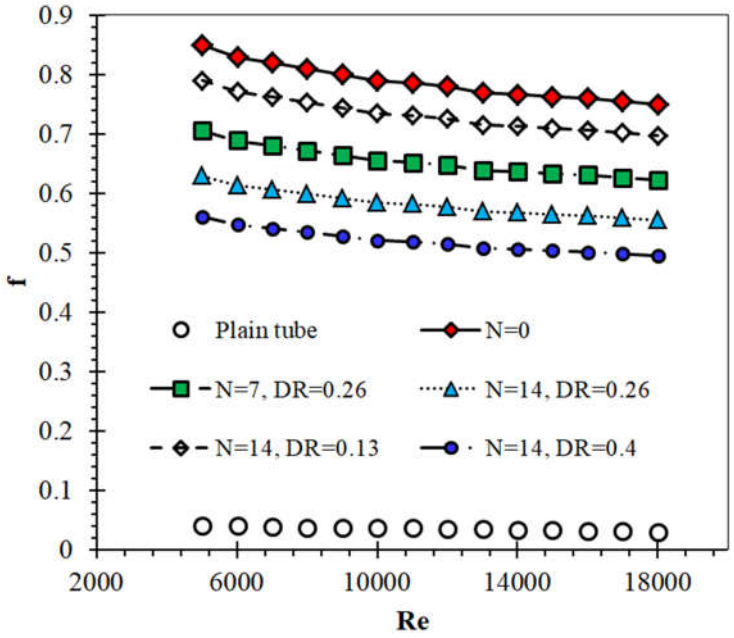

Fig. 11 Variations of the friction loss by Re number for various PVRW inserts with various geometries

Fig. 12 shows the influences of PVRW inserts on the thermohydraulic performance parameter (η) of the turbulent air flows inside heat exchanger pipe. The results indicate that the thermohydraulic performance increases up to 44.2% by using perforated turbulators with N=14 and DR=0.26 in comparison with typical VRW vortex generators (N=0). This augmentation is one of the most important achievements in the present numerical simulations. It can be seen that nearly all of the modified PVRW inserts perform better than the typical VRW inserts. The physical cause for this event is that the additional flow disturbance and swirl flow near the tube walls in much higher in the presence of typical VRWs in comparison with perforated ones. As a result, the friction factor decreases, and the thermohydraulic performance intensified. The use of PVRW turbulators with DR=0.13, 0.26 and 0.40 (at Re=18,000) results in the thermal performance of 1.83, 1.91, 1.58, respectively. It can be seen that the thermohydraulic performance of the heat exchangers equipped with PVRW insert with N=14 and DR=0.26 is the

highest between examined cases and the highest thermal efficiency of $\eta = 2.25$ is reached at Re=5000.

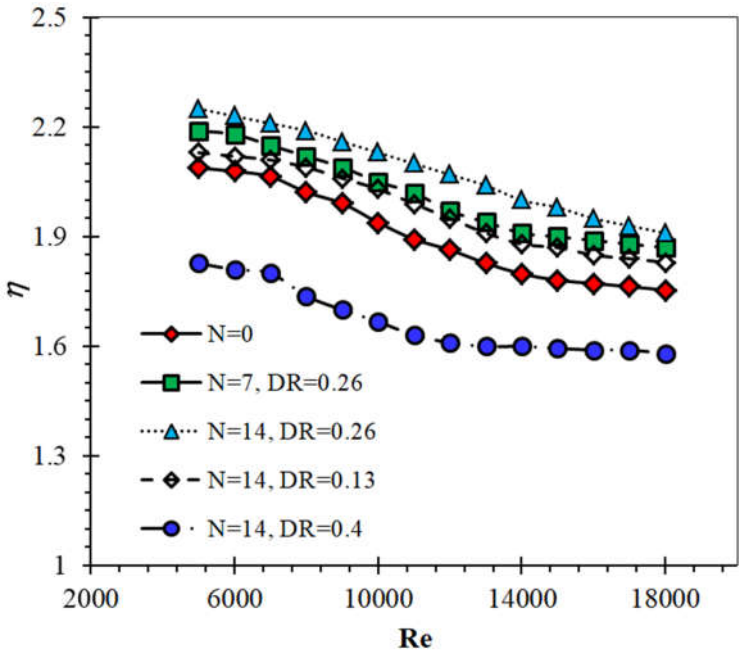

Fig. 12 Variations of thermohydraulic efficiency parameter with Re number for various PVRW inserts with various geometries

Fig. 13 presents a comparison between the thermohydraulic enhancement parameter obtained in the current study for the case of PVRW insert with *N*=14 and *DR*=0.26 with previous experimental and numerical works in the field of vortex generators in heat exchangers with turbulent flow regime. It also should be pointed out to make equal comparisons; the well-known and popular thermal performance factor $\left(\eta = \left(Nu / Nu_s\right) / \left(f / f_s\right)^{1/3}\right)$ is used for calculation of η in this graph. It is noticed that the thermohydraulic performance in the current work is considerably higher than those of the other recent studies with the same Reynolds numbers.

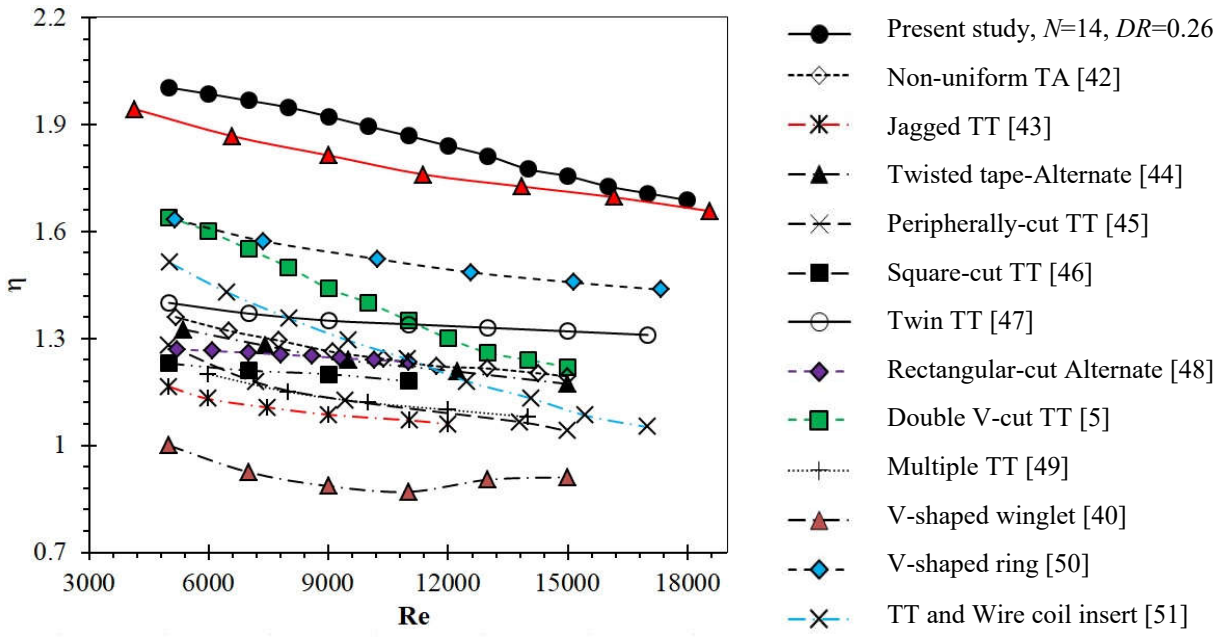

Fig. 13 Comparisons of thermohydraulic efficiency parameter with previous studies

5. Conclusion

In this numerical analysis, the turbulence specifications and thermohydraulic energy efficiency of heat exchangers fitted with perforated V-shaped rectangular winglet vortex generators were evaluated by numerical computations. The Re number was between 5,000 and 18000, the number of holes (*N*) and hole's diameter ratio (*DR*) were in the ranges of 0-14 and 0.13-0.40, respectively. The most important conclusions are as follows:

- The perforated V-shaped vortex generators cause strong recirculating flows between the pipe walls and the tube central regions. The perturbations intensify the fluid mixing, which results in a higher heat transfer rates compared to a heated pipe without any insert.
- The turbulent kinetic energy considerably decreases by using perforated V-shaped rectangular winglet inserts with larger diameter ratios. Increasing the diameter of the

perforations can reduce the recirculation flows and the pressure drop through heat exchanger tubes.

- The average Nusselt number rises by 25.2% with reducing the *DR* from 0.4 to 0.13 at Re=18000 with *N*=14. Moreover, using PVRW inserts with *N*=7, *DR*=0.26, augments the average Nusselt number around 354.3% compared to the simple plain duct without inserts.
- The friction loss decreases by 26.1% by increasing the perforations from 0 to 14 at Re=10,000 and *DR*=0.26. Besides, the friction factor increases by around 51.5% compared to the plain tubes.
- The highest thermal efficiency parameter of $\eta = 2.25$ is obtained at Re=5000 for the heat exchangers enhanced by PVRW insert 14 holes and *DR*=0.26.

References

[1] Chougule, S. S., Sahu, S. K., and Pise, A. T., 2014, "Thermal performance of two phase thermosyphon flat-plate solar collectors using nanofluid," Journal of solar energy engineering, 136(1).

[2] Rashidi, S., Kashefi, M. H., and Hormozi, F., 2018, "Potential applications of inserts in solar thermal energy systems–a review to identify the gaps and frontier challenges," Solar Energy, 171, pp. 929-952.

[3] Hattori, H., Houra, T., Kono, A., and Yoshikawa, S., 2017, "Computational fluid dynamics study for improvement of prediction of various thermally stratified turbulent boundary layers," Journal of Energy Resources Technology, 139(5).

[4] Nakhchi, M. E., and Esfahani, J., 2019, "Sensitivity analysis of a heat exchanger tube fitted with cross-cut twisted tape with alternate axis," Journal of Heat Transfer, 141(4), p. 041902.

[5] Nakhchi, M., and Esfahani, J., 2019, "Numerical investigation of rectangular-cut twisted tape insert on performance improvement of heat exchangers," International Journal of Thermal Sciences, 138, pp. 75-83.

[6] Nakhchi, M., and Esfahani, J., 2018, "Cu-water nanofluid flow and heat transfer in a heat exchanger tube equipped with cross-cut twisted tape," Powder Technology, 339, pp. 985-994.

[7] Xie, G., Li, S., Zhang, W., and Sunden, B., 2013, "Computational fluid dynamics modeling flow field and side-wall heat transfer in rectangular rib-roughened passages," Journal of Energy Resources Technology, 135(4).

[8] Rashidi, S., Akbarzadeh, M., Masoodi, R., and Languri, E., 2017, "Thermal-hydraulic and entropy generation analysis for turbulent flow inside a corrugated channel," International Journal of Heat and Mass Transfer, 109, pp. 812-823.

[9] Akbarzadeh, M., Rashidi, S., and Esfahani, J., 2017, "Influences of corrugation profiles on entropy generation, heat transfer, pressure drop, and performance in a wavy channel," Applied Thermal Engineering, 116, pp. 278-291.

[10] Zhou, J., Hatami, M., Song, D., and Jing, D., 2016, "Design of microchannel heat sink with wavy channel and its time-efficient optimization with combined RSM and FVM methods," International Journal of Heat and Mass Transfer, 103, pp. 715-724.

[11] Tang, W., Hatami, M., Zhou, J., and Jing, D., 2017, "Natural convection heat transfer in a nanofluid-filled cavity with double sinusoidal wavy walls of various phase deviations," International Journal of Heat and Mass Transfer, 115, pp. 430-440.

[12] Nakhchi, M., and Esfahani, J., 2019, "Numerical investigation of turbulent Cu-water nanofluid in heat exchanger tube equipped with perforated conical rings," Advanced Powder Technology, 30(7), pp. 1338-1347.

[13] Nakhchi, M., Esfahani, J., and Kim, K., 2020, "Numerical study of turbulent flow inside heat exchangers using perforated louvered strip inserts," International Journal of Heat and Mass Transfer, 148, p. 119143.

[14] Nakhchi, M., and Esfahani, J., 2020, "Numerical investigation of heat transfer enhancement inside heat exchanger tubes fitted with perforated hollow cylinders," International Journal of Thermal Sciences, 147, p. 106153.

[15] Mosayebidorcheh, S., and Hatami, M., 2018, "Analytical investigation of peristaltic nanofluid flow and heat transfer in an asymmetric wavy wall channel (Part I: Straight channel)," International Journal of Heat and Mass Transfer, 126, pp. 790-799.

[16] Mosayebidorcheh, S., and Hatami, M., 2018, "Analytical investigation of peristaltic nanofluid flow and heat transfer in an asymmetric wavy wall channel (Part II: Divergent channel)," International Journal of Heat and Mass Transfer, 126, pp. 800-808.
[17] Wei Ting, T., Mun Hung, Y., and Guo, N., 2016, "Viscous dissipation effect on streamwise entropy generation of nanofluid flow in microchannel heat sinks," Journal of Energy Resources Technology, 138(5).
[18] Xiong, Q., Bozorg, M. V., Doranehgard, M. H., Hong, K., and Lorenzini, G., 2020, "A CFD investigation of the effect of non-Newtonian behavior of Cu–water nanofluids on their heat transfer and flow friction characteristics," Journal of Thermal Analysis and Calorimetry, 139(4), pp. 2601-2621.
[19] Bozorg, M. V., Doranehgard, M. H., Hong, K., and Xiong, Q., 2020, "CFD study of heat transfer and fluid flow in a parabolic trough solar receiver with internal annular porous structure and synthetic oil–Al2O3 nanofluid," Renewable Energy, 145, pp. 2598-2614.
[20] Hatami, M., Zhou, J., Geng, J., Song, D., and Jing, D., 2017, "Optimization of a lid-driven T-shaped porous cavity to improve the nanofluids mixed convection heat transfer," Journal of Molecular Liquids, 231, pp. 620-631.
[21] Hatami, M., Song, D., and Jing, D., 2016, "Optimization of a circular-wavy cavity filled by nanofluid under the natural convection heat transfer condition," International Journal of Heat and Mass Transfer, 98, pp. 758-767.
[22] Nicodemus, J. H., Huang, X., Dentinger, E., Petitt, K., and Smith, J. H., 2020, "Effects of Baffle Width on Heat Transfer to an Immersed Coil Heat Exchanger: Experimental Optimization," Journal of Energy Resources Technology, 142(5).
[23] Akbarzadeh, M., Rashidi, S., Masoodi, R., and Samimi-Abianeh, O., 2018, "Effect of Transverse Twisted Baffles on Performance and Irreversibilities in a Duct," Journal of Thermophysics and Heat Transfer, pp. 1-14.
[24] Rashidi, S., Akbarzadeh, M., Karimi, N., and Masoodi, R., 2018, "Combined effects of nanofluid and transverse twisted-baffles on the flow structures, heat transfer and irreversibilities inside a square duct–a numerical study," Applied Thermal Engineering, 130, pp. 135-148.
[25] Rashidi, S., Zade, N. M., and Esfahani, J. A., 2017, "Thermo-fluid performance and entropy generation analysis for a new eccentric helical screw tape insert in a 3D tube," Chemical Engineering and Processing: Process Intensification, 117, pp. 27-37.
[26] Zade, N. M., Akar, S., Rashidi, S., and Esfahani, J. A., 2017, "Thermo-hydraulic analysis for a novel eccentric helical screw tape insert in a three dimensional tube," Applied Thermal Engineering, 124, pp. 413-421.
[27] Saravani, M. S., DiPasquale, N. J., Abbas, A. I., and Amano, R. S., 2020, "Heat Transfer Evaluation for a Two-Pass Smooth Wall Channel: Stationary and Rotating Cases," Journal of Energy Resources Technology, 142(6).
[28] Bovand, M., Rashidi, S., and Esfahani, J. A., 2015, "Enhancement of heat transfer by nanofluids and orientations of the equilateral triangular obstacle," Energy conversion and management, 97, pp. 212-223.
[29] Zhou, G., and Ye, Q., 2012, "Experimental investigations of thermal and flow characteristics of curved trapezoidal winglet type vortex generators," Applied Thermal Engineering, 37, pp. 241-248.
[30] Wu, J., and Tao, W., 2011, "Impact of delta winglet vortex generators on the performance of a novel fin-tube surfaces with two rows of tubes in different diameters," Energy conversion and management, 52(8-9), pp. 2895-2901.

[31] Gholami, A., Wahid, M. A., and Mohammed, H., 2014, "Heat transfer enhancement and pressure drop for fin-and-tube compact heat exchangers with wavy rectangular winglet-type vortex generators," International Communications in Heat and Mass Transfer, 54, pp. 132-140.
[32] Song, K., Xi, Z., Su, M., Wang, L., Wu, X., and Wang, L., 2017, "Effect of geometric size of curved delta winglet vortex generators and tube pitch on heat transfer characteristics of fin-tube heat exchanger," Experimental Thermal and Fluid Science, 82, pp. 8-18.
[33] Xu, Y., Islam, M., and Kharoua, N., 2017, "Numerical study of winglets vortex generator effects on thermal performance in a circular pipe," International Journal of Thermal Sciences, 112, pp. 304-317.
[34] Sawhney, J., Maithani, R., and Chamoli, S., 2017, "Experimental investigation of heat transfer and friction factor characteristics of solar air heater using wavy delta winglets," Applied thermal engineering, 117, pp. 740-751.
[35] Salem, M., Althafeeri, M., Elshazly, K., Higazy, M., and Abdrabbo, M., 2017, "Experimental investigation on the thermal performance of a double pipe heat exchanger with segmental perforated baffles," International Journal of Thermal Sciences, 122, pp. 39-52.
[36] Luo, L., Wen, F., Wang, L., Sundén, B., and Wang, S., 2016, "Thermal enhancement by using grooves and ribs combined with delta-winglet vortex generator in a solar receiver heat exchanger," Applied energy, 183, pp. 1317-1332.
[37] Skullong, S., Promthaisong, P., Promvonge, P., Thianpong, C., and Pimsarn, M., 2018, "Thermal performance in solar air heater with perforated-winglet-type vortex generator," Solar Energy, 170, pp. 1101-1117.
[38] Chamoli, S., Lu, R., and Yu, P., 2017, "Thermal characteristic of a turbulent flow through a circular tube fitted with perforated vortex generator inserts," Applied Thermal Engineering, 121, pp. 1117-1134.
[39] Sheikholeslami, M., and Ganji, D., 2016, "Heat transfer improvement in a double pipe heat exchanger by means of perforated turbulators," Energy Conversion and Management, 127, pp. 112-123.
[40] Promvonge, P., and Skullong, S., 2020, "Thermo-hydraulic performance in heat exchanger tube with V-shaped winglet vortex generator," Applied Thermal Engineering, 164, p. 114424.
[41] Nakhchi, M., and Esfahani, J., 2020, "CFD approach for two-phase CuO nanofluid flow through heat exchangers enhanced by double perforated louvered strip insert," Powder Technology, 367, pp. 877-888.
[42] Eiamsa-Ard, S., Somkleang, P., Nuntadusit, C., and Thianpong, C., 2013, "Heat transfer enhancement in tube by inserting uniform/non-uniform twisted-tapes with alternate axes: Effect of rotated-axis length," Applied Thermal Engineering, 54(1), pp. 289-309.
[43] Rahimi, M., Shabanian, S. R., and Alsairafi, A. A., 2009, "Experimental and CFD studies on heat transfer and friction factor characteristics of a tube equipped with modified twisted tape inserts," Chemical Engineering and Processing: Process Intensification, 48(3), pp. 762-770.
[44] Eiamsa-Ard, S., and Promvonge, P., 2010, "Performance assessment in a heat exchanger tube with alternate clockwise and counter-clockwise twisted-tape inserts," International Journal of Heat and Mass Transfer, 53(7-8), pp. 1364-1372.
[45] Eiamsa-ard, S., Seemawute, P., and Wongcharee, K., 2010, "Influences of peripherally-cut twisted tape insert on heat transfer and thermal performance characteristics in laminar and turbulent tube flows," Experimental Thermal and Fluid Science, 34(6), pp. 711-719.

[46] Murugesan, P., Mayilsamy, K., and Suresh, S., 2010, "Turbulent heat transfer and pressure drop in tube fitted with square-cut twisted tape," Chinese Journal of Chemical Engineering, 18(4), pp. 609-617.
[47] Eiamsa-Ard, S., Thianpong, C., and Eiamsa-Ard, P., 2010, "Turbulent heat transfer enhancement by counter/co-swirling flow in a tube fitted with twin twisted tapes," Experimental Thermal and Fluid Science, 34(1), pp. 53-62.
[48] Saysroy, A., Changcharoen, W., and Eiamsa-ard, S., 2018, "Performance assessment of turbular heat exchanger tubes containing rectangular-cut twisted tapes with alternate axes," Journal of Mechanical Science and Technology, 32(1), pp. 433-445.
[49] Piriyarungrod, N., Kumar, M., Thianpong, C., Pimsarn, M., Chuwattanakul, V., and Eiamsa-ard, S., 2018, "Intensification of thermo-hydraulic performance in heat exchanger tube inserted with multiple twisted-tapes," Applied Thermal Engineering, 136, pp. 516-530.
[50] Chingtuaythong, W., Promvonge, P., Thianpong, C., and Pimsarn, M., 2017, "Heat transfer characterization in a tubular heat exchanger with V-shaped rings," Applied Thermal Engineering, 110, pp. 1164-1171.
[51] Promvonge, P., 2008, "Thermal augmentation in circular tube with twisted tape and wire coil turbulators," Energy Conversion and Management, 49(11), pp. 2949-2955.

Figures caption list

Fig. 1 Schematic view of heat exchanger pipe equipped by PVRW turbulators.

Fig. 2 The schematics of the test cases in the present study.

Fig. 3 Typical mesh used in the computational domain.

Fig. 4 Validation of numerical simulations for typical VRW vortex generators with experimental data .

Fig. 5 Flow streamlines inside plain duck and the tube equipped by PVRW turbulators with N=8, DR=0.26 at Re=10,000.

Fig. 6 Contours of turbulent axial velocity in the heat exchangers fitted by typical VRW and PVRW inserts at Re =10000.

Fig. 7 Tangential velocity vectors, TKE contours, and surface flow streamlines inside the duct fitted by VRW inserts at Re=10000.

Fig. 8 TKE contours of fluid flows in heat exchanger ducts improved by different perforated inserts at Re=10,000.

Fig. 9 Temperature contours of turbulent flows through the plain duct and the heat exchanger pipes equipped by different perforated VRWs at Re=10,000.

Fig. 10 Variations of Nu number by Re number for various PVRW turbulators with various geometries.

Fig. 11 Variations of the friction loss by Re number for various PVRW inserts with various geometries.

Fig. 12 Variations of thermohydraulic efficiency parameter with Re number for various PVRW inserts with various geometries.

Fig. 13 Comparisons of thermohydraulic efficiency parameter with previous studies.

Tables caption list

Table 1 Dimensions of the design parameters inside heat exchanger pipe equipped with PVRW vortex generators.

Table 2 Grid independence study for PVRW turbulator at Re = 18,000, N=14, DR =0.4.